Oil Shale, 2012, Vol. 29, No. 1, pp. 18–35
doi: 10.3176/oil.2012.1.03
ISSN 0208-189X


# SEA-LEVEL CHANGES RECORDED BY CERIUM ANOMALIES IN THE LATE JURASSIC (TITHONIAN) BLACK ROCK SERIES OF QIANGTANG BASIN, NORTH-CENTRAL TIBET

LAN CHEN [(a,b,d)*], ANDREW TIEN-SHUN LIN[(b)], XUEJUAN DA[(a)], HAISHENG YI[(c)], LOUIS LOUNG-YIE TSAI[(d)], GUIWEN XU[(a)]

[(a)] College of Petroleum Engineering
Chongqing University of Science and Technology
Chongqing 401331, China

[(b)] Institute of Geophysics
National Central University
Jhongli 32001, Taiwan, R.O.C

[(c)] Institute of Sedimentary Geology
Chengdu University of Technology
Chengdu 610059, China

[(d)] Institute of Applied Geology
National Central University
Jhongli 32001, Taiwan, R.O.C

*The Upper Jurassic black rock series of the Amdo area of north-central Tibet have attracted attention because of its organic-rich matter and oil seepage in the rock series. Abundant ammonites of Aulacosphinctes and Virgatosphinctes as well as bivalves including Buchia and Chlamys, are well preserved in the Qiangmuleiqu Formation of the Middle to Late Tithonian (Late Jurassic). The total rare earth elements (∑REE) abundance of the formation varies from 18.814 to 46.818 ppm and is lower than that of an average in marine shales. Inter-element correlations suggest that the shale-normalized REE patterns provide the information about the origin of sedimentary rocks (i.e., not affected by diagenesis), and can be used as a potential indicator for eustatic sea-level changes. The $Ce_{anom}$ values gradually increased from –0.015 to –0.238 from the lower to middle part of the series, indicating a rise in sea level. The $Ce_{anom}$ then dropped to –0.081, suggesting a lowering of sea level. From the middle to upper part of the section, there are two more sea-level fluctuations indicated by variations of cerium anomaly values. Thus, sea-level fluctuations occurred three times in this Late Jurassic section, with major episodes of eustatic rise took place in the lower-middle part of this section. These episodic cycles show*

* Corresponding author: e-mail *cllc-10@163.com*

*that the sediments in the Amdo area of north-central Qiangtang basin were deposited in continental shelf or deep-water continental slope environments, which is not in agreement with the previous views that there are no deep-water sediments in Qiangtang basin. Our results call for further studies to be undertaken on Jurassic stratigraphic framework and tectono-sedimentary evolution in Qiangtang basin, northern Tibet.*

## Introduction

Sea-level fluctuations have important implications for organic productivity of the oceans and sediment distribution patterns along the continental margins and in the interior basins [1]. Therefore, the study of these fluctuations is of prime interest to hydrocarbon exploration. Sea-level changes are also thought to control hydrographic-climatic patterns and, indirectly, biotic distribution patterns as well [1–5]. Understanding these changes is of considerable value in deciphering past oceanographic (palaeoceanographic) conditions [1]. Advances in seismic stratigraphy, sequence stratigraphy and the development of depositional models have provided the basis for the recognition of sea-level events in subsurface data and in outcrops of marine sediments around the world [6–13]. However, these traditional methods cannot provide quantitative and continuous curves of sea-level changes in the Phanerozoic. A possible independent method for determining relative sea level, for specific geologic situations, is suggested by the use of the cerium anomaly as part of a chemostratigraphic study [14–16].

In recent years, much attention has been paid to the behaviour of cerium (Ce), and particularly the Ce-anomaly in the marine environment, for understanding the palaeoceanographic conditions [17–23]. Ce anomaly has also been used as a potential indicator of eustatic sea-level changes [15, 24] (except for the redox conditions [15, 19, 25–27]), tectonic reconstruction [28] and diagenetic process [18]. Ce has two possible oxidation states: $Ce^{3+}$ and $Ce^{4+}$. In oxic conditions, Ce is less readily dissolved in seawater, which shows negative Ce anomaly (<–0.1) of $\log[3Ce_n/(2La_n+Nd_n)]$ [29]. Oxic sediments on the other hand are more enhanced with respect to Ce and show less negative to positive Ce anomaly (>–0.1) [14]. Conversely, anoxic water would have positive Ce anomalies and anoxic sediments would show negative anomalies. Therefore, changes in the value of the anomaly could be related to redox conditions predicted by the ventilation model of Wilde [30], with more negative values found during warmer climates and transgressive conditions and more positive values found during cooler to glacial climates and regressive conditions. Thus, whole-rock cerium anomaly is a geochemical parameter that characterizes chemical palaeoceanographic conditions related to relative sea-level changes independent of sedimentological or seismic considerations [15]. Furthermore, the use of a chemical parameter offers the possibility of the extension of its interpretation to quantitative palaeoenvironmental studies beyond that of sea-level curves.

Although the Qiangtang Basin of north Tibet has arguably the most complete and extensive marine sedimentary strata of the Jurassic period [31], its ammonites zones or subzones of Early to Late Jurassic have not been well established. Previous studies have shown that only a few ammonites have been found in the Shuanghu-Sewa-Amdo area and the geographic distribution of ammonite fauna can be potentially associated with sea-level rise [32–33]. In this study we present Ce anomaly determinations from late Jurassic ammonites found in black shales of the Amdo Highway 114 station, southern Qiangtang basin. Combined with the published palaeontological data [32–35], we discuss the Late Jurassic sea-level changes and geological significance of the black rock series in the Amdo area, northern Tibet.

## Geologic setting

The black rock series for this study come from exposures in Gangni village (Township) and Amdo 114 station (of the Qinghai-Tibet highway), north-central Tibet (Fig. 1). Rocks mainly consist of black shales, dark grey calcareous mudstones and marls with abundant ammonites of Jurassic, which are significantly different from the Yanshiping Group biological assemblage and/or sedimentary characteristics. The Gangni Township section yields ammonites of Sonninidae, mainly including *Sonninia*, *Dorsetensia*, *Witchellia*, etc., and belonging to the Early to Middle Bajocian (Middle Jurassic) [34].

The section near the Amdo 114 station has been noticed by many geologists because of oil seepage. This section is located at long. 91°47′ W,

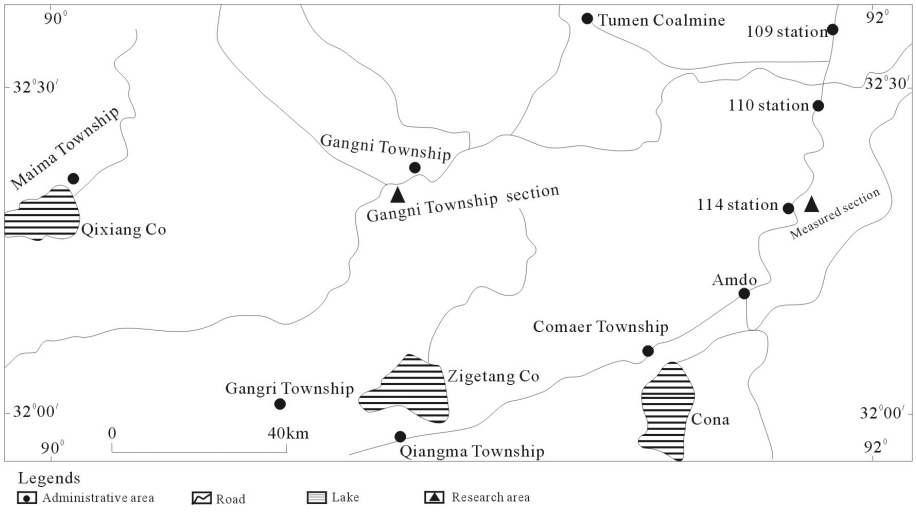


*Fig. 1.* Location of the stratigraphic sections outcropping Jurassic black rock series with ammonites at Gangni village and the Amdo Highway 114 station, Amdo county, Qiangtang basin of northern Tibet.

lat. 32°26′ N (Fig. 1). Jiang [36] named it Qiangmuleiqu Formation ($J_3q$). The strata are of west-east strike and dipping 60° to 70°southward. The whole succession is divided into three intervals characterized by different lithological types. The lower part of this section is about 134 m thick and outcrops in the core of an anticline. Rocks in the lower part consist in general of mauve sandstones, siltstones and greyly green siltstones interbedded with a few intercalated mud boulder horizons. Continuous black sedimentation of limestones, bioclastic and silty limestones occurred in the middle interval. The upper part of the section is divided into two members. The lower member, about 75 m thick, developed greyish green siltstones and calcareous fine sandstones with intercalated argillaceous siltstones and silty mudstones, whereas, the upper member, about 296 m thick, is of abundant ammonite fauna and mainly deposited as grey marls and greyish black calcareous mudstones with cycles. Its horizon is indicated by oil seepage. The top of this section is covered by Quaternary sediments.

Because of its excellent exposure and easy access, the Amdo 114 station section is well known and probably the best studied locality of Late Jurassic strata in the northern Qiangtang basin, Tibet. Additionally, the section mainly consists of abundant fossils, such as ammonites, bivalves and brachiopods. Recent results show this section mainly consists of 7 genus and 7 species in ammonites, 3 genera and 1 species in bivalves, and 1 genus and 1 species in brachiopods. Most of the ammonites belong to Virgatosphinctinae subfamily, mainly including *Aulacosphinctes*, *Virgatosphinctes*, the Berriasellinae subfamily, with *blanfordiceras*, and Spiticeratinae subfamily with *Spiticeras* (Fig. 2). Above observed ammonites are more classic fossils of Middle-Late Tithonian (Late Jurassic). It is well known that the *Aulacosphinctes* occurred wildly in Himalaya of China, southeast France, Denmark, Madagascar, Kachchh district in Gujarat state, India, and Nepal [33, 37-38] and can be correlated with the Spiti ammonites in the western Himalayan region, while the *Virgatosphinctes* yielded the whole world [39]. In addition, bivalves were found throughout the section including *Buchia* and *Chlamys*. It is difficult to compare these ammonoid assemblages with the European standards because of the absence of respective data. However, it is realistic to make a regional biochronologic correlation with other ammonoid successions of Spiti Shales in western Himalayan region, or Bailongbinghe Formation in the north Qiangtang basin, or Hongqilapu Formation in Karakorum area, or Menkadun Formation in Everest area, south Tibet [32, 40].

## Material and methods

We carried out detailed investigations of the Upper Jurassic black shales of the Amdo 114 station section, Qiangtang basin of northern Tibet. This 650 m thick section was studied bed by bed with the vertical sample spacing of

29 m on the average (22 samples in total) (Fig. 2). On each bed, samples are palaeoecological and/or palaeoceanographic interpretations. The analysis of rare earth elements (REE) has been carried out by a Perkin-Elmer Sciex

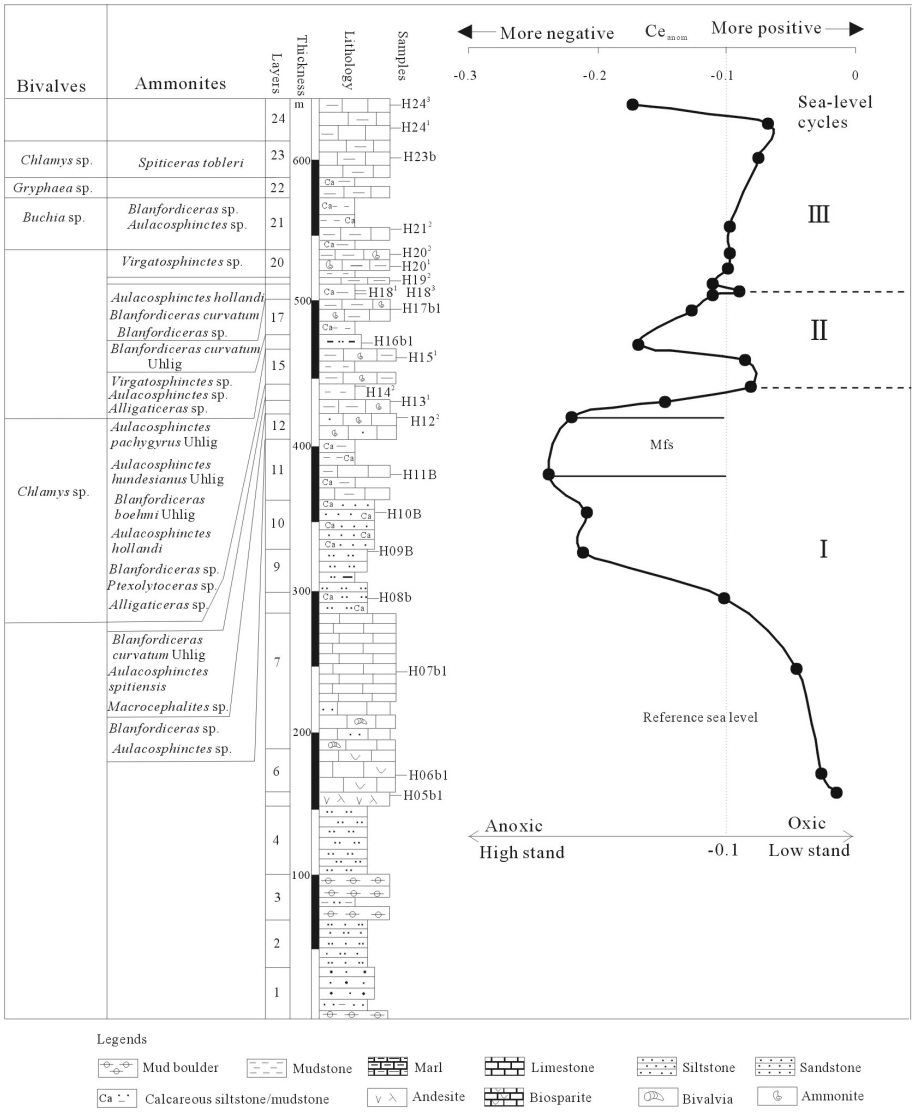


*Fig. 2.* The lithostratigraphy and cerium anomalies in the Amdo 114 station, Qiangtang basin of northern Tibet. Abundant ammonites occurred upwards starting from the layer No. 12, mainly dominated by *Aulacosphinctes*, *Virgatosphinctes*. Bivalves (*Chlamys*, *Gryphaea*, and *Buchia)* occurred only on the layers No. 15, 21, 22, 23 and 24 belonging to Middle-Late Tithonian. The curve of Cerium anomaly fluctuates distinctively between more positive and more negative Cerium anomalies from lower to upper layers, and three cycles of eustatic sea-level rise and fall can be distinguished.

taken less attention. We also collected samples for isotopic dating (Re-Os and Pb-Pb), in order to obtain a comprehensive database for strata ages, ELAN 6000 inductively coupled plasma mass spectrometer (ICP-MS) at the dark to black color, higher argillaceous sediments, so the lower part was State Key Laboratory of Ore Deposit Geochemistry, Institute of Geochemistry, Chinese Academy of Sciences, using fully quantitative solution analysis methods described earlier [41–43]. The international reference standards OU-6 and AHM-1 were used to check the analytical accuracy. Analytical uncertainties are better than 5% for all elements based on the reproducibility of standards.

## Results and discussion

Bulk concentration of REE abundance of sediments from the Amdo 114 station section is presented in Table 1, and the correlation coefficient values ($\gamma$) among REE are listed in Table 2 by Pearson's mathematical formula. The Post Archean Australian Shale (PAAS)-normalized REE pattern of the sediments is presented in Fig. 3 to understand their behaviors. The Ce anomaly values vary from –0.238 to –0.015 and exhibit the eustatic sea-level changes (Fig. 2).

### REE concentrations

Total concentrations of REE's of the Upper Jurassic black rock series stay between 18.814 and 46.818 ppm (Table 1), except for two samples (H06b1 and H07b1) having REE's concentration <10 ppm and one sample (H05b1) having REE's concentration >100 ppm. Concentrations are lower than those of the average shales from Turekian and Wedepohl [44]. We calculated the ∑LREE/∑HREE (∑light rare earth elements / ∑heavy rare earth elements) as (La+Ce+…+Eu)/(Gd+Tb+…+Lu) and their ratios vary from 6.6 to 9.4 (except for sample H05b1 having ratio of 17.214) and show a positive correlation with La/Yb ($\gamma = 0.7$). In addition, the other REEs show good positive correlations. Cerium and the trivalent REEs represented by La indicate similar correlation coefficient value ($\gamma = 0.974$) with Sm whereas Eu is correlated with La (0.986) and Ce (0.989). On the other hand Ce is not better correlated with Lu (0.569) than La (0.644) (Table 2). The stronger positive correlations show that the REE concentrations may represent original sedimentary information not reflected by diagenetic constraints: thus the REE concentrations can be used for a potential indicator as eustatic sea-level changes [16, 19]. The shale-normalized [45] REE patterns are characterized by the flat shale type with unstable Ce anomalies and very weak positive Eu anomalies. Furthermore, the lower part of this section shows distinctly different REE pattern from the middle and upper part. Sample H05b1 is an andesite and has a significant left-toward trend, while the samples H06b1 and H07b1 are limestones and have a lightly flat type

*Table 1.* **REE concentrations (ppm) with Ce and Eu anomaly values of the Upper Jurassic black rock series in the Amdo 114 station, northern Tibet**

| Sample | Lithology | La | Ce | Pr | Nd | Sm | Eu | Gd | Tb | Dy | Ho |
|---|---|---|---|---|---|---|---|---|---|---|---|
| H24[3] | argillaceous limestone | 3.586 | 4.717 | 0.663 | 2.608 | 0.508 | 0.114 | 0.542 | 0.080 | 0.473 | 0.114 |
| H24[1] | argillaceous limestone | 7.056 | 11.977 | 1.418 | 5.363 | 1.066 | 0.235 | 1.049 | 0.155 | 0.870 | 0.200 |
| H23b | argillaceous limestone | 7.511 | 12.465 | 1.530 | 5.612 | 1.014 | 0.228 | 0.966 | 0.142 | 0.832 | 0.197 |
| H21[2] | marl | 7.877 | 12.350 | 1.584 | 5.766 | 1.047 | 0.239 | 1.044 | 0.163 | 0.947 | 0.222 |
| H20[2] | marl | 9.273 | 14.352 | 1.735 | 6.521 | 1.318 | 0.284 | 1.221 | 0.190 | 1.152 | 0.255 |
| H20[1] | marl | 9.278 | 14.602 | 1.835 | 6.955 | 1.429 | 0.285 | 1.322 | 0.207 | 1.144 | 0.248 |
| H19[2] | marl | 9.861 | 14.783 | 1.872 | 6.912 | 1.324 | 0.289 | 1.199 | 0.202 | 1.062 | 0.253 |
| H18[3] | calcareous mudstone | 11.256 | 17.932 | 2.301 | 8.199 | 1.633 | 0.330 | 1.444 | 0.240 | 1.329 | 0.309 |
| H18[1] | calcareous mudstone | 9.831 | 14.777 | 1.842 | 6.922 | 1.272 | 0.301 | 1.272 | 0.222 | 1.182 | 0.271 |
| H17b1 | marl | 8.466 | 12.152 | 1.577 | 5.772 | 1.148 | 0.253 | 1.088 | 0.168 | 0.997 | 0.221 |
| H16b1 | silty mudstone | 9.514 | 12.233 | 1.618 | 6.172 | 1.140 | 0.259 | 1.144 | 0.173 | 0.995 | 0.228 |
| H15[1] | marl | 11.460 | 18.197 | 2.205 | 8.021 | 1.515 | 0.339 | 1.414 | 0.224 | 1.350 | 0.283 |
| H14[2] | mudstone | 9.109 | 14.819 | 1.825 | 6.624 | 1.374 | 0.313 | 1.329 | 0.209 | 1.148 | 0.257 |
| H13[1] | marl | 9.171 | 12.469 | 1.653 | 6.091 | 1.150 | 0.241 | 1.189 | 0.182 | 0.958 | 0.227 |
| H12[2] | limestone | 9.883 | 11.183 | 1.617 | 6.212 | 1.106 | 0.235 | 1.135 | 0.189 | 1.032 | 0.226 |
| H11B | marl | 6.529 | 6.993 | 1.064 | 3.880 | 0.709 | 0.163 | 0.745 | 0.125 | 0.639 | 0.175 |
| H10B | calcareous sandstone | 6.275 | 7.314 | 1.046 | 3.941 | 0.730 | 0.167 | 0.823 | 0.125 | 0.646 | 0.164 |
| H09B | siltstone | 6.368 | 7.436 | 1.045 | 4.171 | 0.717 | 0.168 | 0.729 | 0.123 | 0.681 | 0.175 |
| H08b | calcareous siltstone | 4.533 | 7.056 | 0.865 | 3.337 | 0.708 | 0.159 | 0.677 | 0.101 | 0.530 | 0.138 |
| H07b1 | cryptite | 0.800 | 1.471 | 0.171 | 0.672 | 0.135 | 0.030 | 0.131 | 0.020 | 0.126 | 0.025 |
| H06b1 | biosparite | 2.214 | 4.150 | 0.458 | 1.716 | 0.318 | 0.076 | 0.316 | 0.049 | 0.225 | 0.047 |
| H05b1 | andesite | 23.926 | 45.318 | 4.957 | 17.431 | 2.958 | 0.707 | 2.191 | 0.297 | 1.330 | 0.269 |
| Average | | 8.353 | 12.670 | 1.585 | 5.859 | 1.105 | 0.246 | 1.044 | 0.163 | 0.893 | 0.205 |
| Average shale | | 92.000 | 59.000 | 5.600 | 24.000 | 6.400 | 1.000 | 6.400 | 1.000 | 4.600 | 1.200 |
| OU-6 | True | 33 | 74.42 | 7.8 | 29.01 | 5.92 | 1.36 | 5.27 | 0.85 | 4.99 | 1.01 |
| | Measured | 32.162 | 73.31 | 7.69 | 28.58 | 5.763 | 1.316 | 5.13 | 0.836 | 4.913 | 1.074 |
| AHM-1 | True | 15.87 | 33.03 | 4.21 | 17.69 | 3.68 | 1.16 | 3.34 | 0.51 | 2.84 | 0.57 |
| | Measured | 15.217 | 31.545 | 4.065 | 15.817 | 3.404 | 1.079 | 3.184 | 0.513 | 2.646 | 0.574 |

| Sample | Lithology | Er | Tm | Yb | Lu | ∑REE | ∑LREE/∑HREE | $La_n/Sm_n$ | Pr/Pr* | $Ce_{anom}$ | Eu/Eu* |
|---|---|---|---|---|---|---|---|---|---|---|---|
| H24[3] | argillaceous limestone | 0.289 | 0.041 | 0.243 | 0.039 | 14.016 | 6.699 | 1.026 | 1.103 | –0.173 | 1.026 |
| H24[1] | argillaceous limestone | 0.520 | 0.074 | 0.488 | 0.075 | 30.544 | 7.906 | 0.962 | 1.041 | –0.068 | 1.047 |
| H23b | argillaceous limestone | 0.522 | 0.071 | 0.474 | 0.069 | 31.632 | 8.664 | 1.077 | 1.075 | –0.075 | 1.084 |
| H21[2] | marl | 0.661 | 0.077 | 0.500 | 0.072 | 32.549 | 7.831 | 1.093 | 1.103 | –0.097 | 1.078 |
| H20[2] | marl | 0.677 | 0.090 | 0.540 | 0.088 | 37.696 | 7.948 | 1.022 | 1.055 | –0.098 | 1.055 |
| H20[1] | marl | 0.692 | 0.098 | 0.618 | 0.095 | 38.808 | 7.773 | 0.943 | 1.069 | –0.099 | 0.978 |
| H19[2] | marl | 0.712 | 0.087 | 0.613 | 0.080 | 39.247 | 8.330 | 1.082 | 1.088 | –0.111 | 1.079 |
| H18[3] | calcareous mudstone | 0.845 | 0.121 | 0.774 | 0.105 | 46.818 | 8.061 | 1.001 | 1.116 | –0.090 | 1.013 |
| H18[1] | calcareous mudstone | 0.723 | 0.088 | 0.632 | 0.082 | 39.417 | 7.816 | 1.123 | 1.070 | –0.111 | 1.113 |
| H17b1 | marl | 0.573 | 0.077 | 0.522 | 0.067 | 33.081 | 7.911 | 1.071 | 1.106 | –0.127 | 1.067 |
| H16b1 | silty mudstone | 0.599 | 0.084 | 0.526 | 0.069 | 34.752 | 8.102 | 1.213 | 1.091 | –0.169 | 1.066 |
| H15[1] | marl | 0.786 | 0.115 | 0.688 | 0.096 | 46.694 | 8.421 | 1.099 | 1.074 | –0.086 | 1.092 |
| H14[2] | mudstone | 0.712 | 0.098 | 0.636 | 0.083 | 38.536 | 7.617 | 0.963 | 1.083 | –0.081 | 1.090 |
| H13[1] | marl | 0.582 | 0.081 | 0.504 | 0.076 | 34.574 | 8.101 | 1.159 | 1.113 | –0.147 | 0.972 |
| H12[2] | limestone | 0.593 | 0.085 | 0.495 | 0.063 | 34.055 | 7.919 | 1.298 | 1.131 | –0.221 | 0.989 |
| H11B | marl | 0.459 | 0.059 | 0.370 | 0.050 | 21.959 | 7.374 | 1.339 | 1.191 | –0.238 | 1.054 |
| H10B | calcareous sandstone | 0.436 | 0.055 | 0.363 | 0.050 | 22.134 | 7.315 | 1.250 | 1.138 | –0.208 | 1.013 |
| H09B | siltstone | 0.451 | 0.059 | 0.339 | 0.046 | 22.506 | 7.648 | 1.291 | 1.093 | –0.212 | 1.093 |
| H08b | calcareous siltstone | 0.331 | 0.043 | 0.294 | 0.042 | 18.814 | 7.727 | 0.931 | 1.047 | –0.101 | 1.080 |
| H07b1 | cryptite | 0.080 | 0.007 | 0.063 | 0.009 | 3.741 | 7.105 | 0.858 | 1.013 | –0.047 | 1.063 |
| H06b1 | biosparite | 0.134 | 0.023 | 0.140 | 0.018 | 9.883 | 9.393 | 1.011 | 1.010 | –0.027 | 1.133 |
| H05b1 | andesite | 0.694 | 0.083 | 0.598 | 0.074 | 100.832 | 17.214 | 1.175 | 1.036 | –0.015 | 1.307 |
| Average | | 0.549 | 0.073 | 0.474 | 0.066 | 33.286 | 8.313 | 1.090 | | –0.118 | 1.068 |
| Average shale | | 2.500 | 0.200 | 2.600 | 0.700 | | | | | | |
| OU-6 | True | 2.98 | 0.44 | 3 | 0.45 | | | | | | |
| | Measured | 3.072 | 0.448 | 3.196 | 0.473 | | | | | | |
| AHM-1 | True | 1.52 | 0.21 | 1.37 | 0.21 | | | | | | |
| | Measured | 1.479 | 0.209 | 1.393 | 0.2 | | | | | | |

*Table 2.* **Pearson's correlation coefficients of REEs for all samples in the Amdo 114 station, Qiangtang basin in northern Tibet**

| | La | Ce | Pr | Nd | Sm | Eu | Gd | Tb | Dy | Ho | Er | Tm | Yb | Lu |
|---|---|---|---|---|---|---|---|---|---|---|---|---|---|---|
| La | 1 | | | | | | | | | | | | | |
| Ce | 0.974 | 1 | | | | | | | | | | | | |
| Pr | 0.991 | 0.994 | 1 | | | | | | | | | | | |
| Nd | 0.994 | 0.990 | 0.999 | 1 | | | | | | | | | | |
| Sm | 0.981 | 0.974 | 0.988 | 0.990 | 1 | | | | | | | | | |
| Eu | 0.986 | 0.989 | 0.995 | 0.995 | 0.993 | 1 | | | | | | | | |
| Gd | 0.955 | 0.913 | 0.945 | 0.954 | 0.977 | 0.959 | 1 | | | | | | | |
| Tb | 0.905 | 0.839 | 0.885 | 0.897 | 0.932 | 0.903 | 0.981 | 1 | | | | | | |
| Dy | 0.810 | 0.730 | 0.785 | 0.801 | 0.854 | 0.812 | 0.933 | 0.973 | 1 | | | | | |
| Ho | 0.756 | 0.657 | 0.723 | 0.741 | 0.797 | 0.751 | 0.894 | 0.951 | 0.984 | 1 | | | | |
| Er | 0.727 | 0.634 | 0.700 | 0.716 | 0.775 | 0.727 | 0.873 | 0.938 | 0.979 | 0.993 | 1 | | | |
| Tm | 0.668 | 0.570 | 0.639 | 0.656 | 0.727 | 0.666 | 0.836 | 0.903 | 0.966 | 0.973 | 0.977 | 1 | | |
| Yb | 0.718 | 0.637 | 0.699 | 0.714 | 0.781 | 0.728 | 0.876 | 0.937 | 0.976 | 0.984 | 0.987 | 0.983 | 1 | |
| Lu | 0.644 | 0.569 | 0.629 | 0.646 | 0.725 | 0.661 | 0.829 | 0.887 | 0.951 | 0.961 | 0.966 | 0.975 | 0.974 | 1 |

(Fig. 3c) with a positive cerium anomaly. The middle and upper part is identified by flat shale type rock with significantly negative cerium anomaly (Fig. 3a, 3b). Major changes in REE composition and abundance can be seen in samples H05b1, H06b1 and H07b1, which show that basal samples have low concentration of REEs, whereas the remaining layers are abundant in REEs compared to the underlying strata. The relatively flat pattern of REE concentrations indicates a detrital origin and good mixing during transportation [46].

The Ce concentration in the bulk shales and phosphorite is generally determined by detrital constituents like clays and organic matter, hence, in most shales or phosphorites, the La/Sm ratio increases and the Ce anomaly diminishes with the increase of detrital fraction [46]. Ce anomalies with flat REE distribution and (La/Sm)n ratios >0.35 could be used as indication of oceanic anoxia [20, 23, 47]. All samples with (La/Sm)n ratios >0.858–1.339 do not have correlation with Ce anomaly, which indicates that diagenesis has no effect on the values of true Ce anomaly. Bau and Dulski [48] discussed the La and Ce anomalies by looking additionally at praseodymium $Pr/Pr^*$ values using the equation $Pr/Pr^* = 2Pr_n/(Ce_n+Nd_n)$. The existence of a true Ce anomalies should lead to $Pr/Pr^* \geq 1$. If, however, samples show $Pr/Pr^* = 1$, this would imply that anomalous La enrichment must be the sole cause of any $Ce_{anom}$. As shown in Table 1, the average $Pr/Pr^*$ ratio is 1.084 in the Amdo 114 station, which indicates that these Ce anomaly differences are subtle and may have been artificially enhanced by different La concentrations [48]. The $Ce_{anom}$ values vary from –0.238 to –0.015, whereas $Eu/Eu^*$ values (using the equation $Eu/Eu^* = Eu_n/(Sm_n \times Gd_n)^{0.5}$ [49]), vary from 0.972 to 1.133.

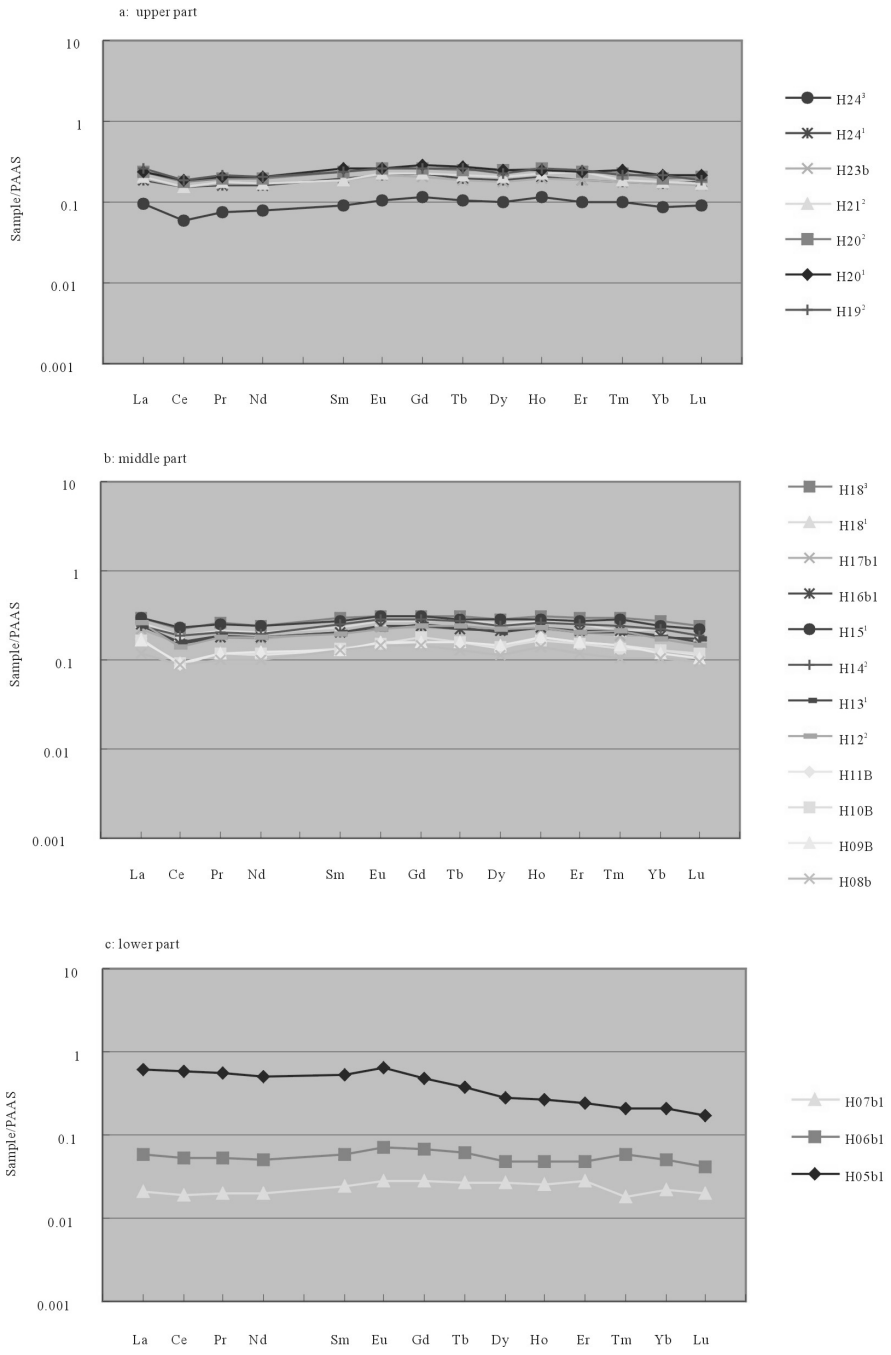


*Fig. 3.* Shale-normalized REE distribution of Upper Jurassic black rock series from the Amdo 114 station in northern Tibet. The upper part (a) has weakly negative cerium anomaly and represents the third sea-level cycle, while the middle part (b) shows more negative cerium anomalies from H08b to $H18^3$ corresponding to the first and second sea-level cycles. The lower part (c) is characterized by weakly positive to positive cerium anomalies. Sample H05b1 is different from others (a, b).

## Cerium anomaly as an indicator of sea-level change

*Geochemistry of cerium*

The use of the cerium anomaly was first proposed by Elderfield and Greaves [29] as a consequence of the change in the ionic state of Ce as a function of oxidation state. The removal of dissolved Ce (+3) as insoluble form of Ce (+4) preferentially occurs in the upper part of the water column, so oxic seawater shows a negative Ce anomaly, whereas oxic sediments have a less negative to a positive value [14]. Conversely, in anoxic sediments, Ce is released and the sediments show a negative anomaly. Most of the black shales, Cambrian chert-phosphorite assemblages, fossil apatite discussed during past years have a positive cerium anomaly associated with anoxic sediments during warmer climate and transgressive conditions [14–15, 46, 50]. In other words, the observed Ce anomaly is not limited to marine carbonate, conodonts and ichthyoliths, while the whole-rock Ce anomaly can be used as an indicator of intensity of anoxia and therefore of eustatic sea-level. A positive-trending whole-rock cerium anomaly indicates more oxic conditions or a sea-level fall. In contrast, negative-trending anomaly indicates more reducing conditions or a sea-level rise [15]. Ce anomaly methods have been applied for the Middle Ordovician to Early Silurian quantitative sea-level curve at Dob's Linn, Scotland [15] and in the study of Chinese seawater from the Sinian to the early Cambrian in the Yangtze Region [51].

*Sea-level change*

Table 1 and Fig. 2 show the cerium anomaly changes obtained in this study. The highest $Ce_{anom}$ value (–0.015 of H05b1) is in the lower part and gradually decreases in the middle part. The $Ce_{anom}$ values fell down to the lowest (–0.238 of H11B), then rose rapidly to about –0.1. The relatively stable values occurred in the upper part, but the values changed from –0.075 to –0.173 in the argillaceous limestones in the top part. Three cycles of the relative sea-level fall and rise were identified based on Ce anomalies in the Amdo 114 station (Fig. 2).

Cycle I occurred in the lower and middle parts of this section (from samples H05b1 to H14[2]) showing positive to slightly negative Ce anomaly for the whole-rock. During a transgression the bottom waters became more anoxic. The sample H05b1 with the highest $Ce_{anom}$ value indicates that sea-level surface fell to the lowest, then from samples H05b1 to H08b, the relative sea-level began to rise gradually as can be seen from dropping value of $Ce_{anom}$. At 370 m, the $Ce_{anom}$ value (–0.238) decreased to the lowest, indicating the sea-level changes are maximum flooding surface (Mfs) until at 420 m (Fig. 2). Additionally, during the transgressive process, the abundant ammonites including *Blanfordiceras* sp. and *Aulacosphinctes* sp. were found. Yin and Enay [32] discussed the reasons why such Tithonian ammonites of Gondwana facies suddenly occurred in northern Tibet (for

example, the palaeoclimate, tectonic framework and palaeogeography changes). As mentioned above, the occurrence of *Blanfordiceras* sp. and *Aulacosphinctes* sp. may indicate the extension of the Himalayan marine basin and sea-level rise, so this fauna is interpreted as a marker of the deeper water outer shelf or continental slope [32, 40]. Subsequently, the sea level began to fall slowly into the Cycle II.

After the Cycle I, the relative sea-level began to rise with slightly negative $Ce_{anom}$ values between –0.081 and –0.169, and fall at the beginning of about 465 m. As shown in Fig. 2, the Cycle II mainly occurred in the greyly black, dark grey marls, limestones, mudstones, or calcareous mudstones with abundant ammonites. In particular, the grey marls of layer No. 15 are characterized by ammonites as follows: *Aulacosphinctes pachygyrus* (Uhlig), *Aulacosphinctes hundesianus* (Uhlig), *Blanfordiceras boehmi* (Uhlig), *Blanfordiceras* sp., *Aulacosphinctes Hollandi, Alligaticeras* sp., and *Ptexolytoceras* sp. (Fig. 2). In addition, the *Virgatosphinctes* sp. occurs for the first time in No. 16 bed. The above-mentioned ammonites of *Aulacosphinctes* and *Virgatosphinctes* generally lived in the outer shelf and upper slope [32, 37, 52].

Sea-level stillstand followed by the Cycle II and the $Ce_{anom}$ values very close to –0.10, probably indicate a weakly oxic environment. At the beginning of the Cycle III, there are no distinct cerium anomalies. Ce anomalies then are lower than –0.10 and show a gradual increasing trend at about 600 m, indicating enhanced oxidizing conditions in seawater and sea-level fall. In the upper part of this section, light grey marls, yellow grey marls and calcareous mudstones formed with the ammonite fossils of *Spiticeras tobleri,* which is regarded as the latest Tithonian. In the Himalayan region, the Late Jurassic is marked by the deep marine Spiti Shales [37, 39], which showed the transition of continental shelf to slope.

The Tithonian part of the eustatic sea-level curve of Haq et al. [1] shows several unusually rapid oscillations. Hallam [53] argued that this was rather a consequence of tensional tectonic activity, producing rotated fault blocks. Both Haq et al. [1] and Hallam [53] agree that the Tithonian marked a sea-level peak and was followed by a fall into the earliest Cretaceous. According to the relationship between the Ce anomaly and the eustatic sea-level curve from the Amdo 114 station in northern Tibet (Fig. 2), we identified the Late Jurassic sea-level changes. Changes in the Ce anomaly that are positive would indicate a lowering of sea-level as the apparent depth. Negative relative changes would indicate a rise in sea level. Thus, we can conclude that the deepest sea-water occurred in the middle part of the section, which is in consistent with the appearance of abundant ammonites. According to the results of analysis we assume that formation of the Upper Jurassic black rock series may be controlled by sea-level fluctuations.

## Geological implications

*Age of studied section*

Upper Jurassic marine strata of northern Tibet were first reported by Fan et al. [54] who found ammonites, bivalves, and corals in Gaze area of north-western Tibet. Upper Jurassic strata with abundant ammonites only outcropped at the Amdo 114 station in Amdo county of north-central Tibet. However, due to a small sample size, poor or even erroneous stratigraphic control, as well as inadequate identification of the previous collections, the previous studies failed to establish well-defined levels of ammonoid genera or assemblages. Although the Tithonian sediments are mostly fossiliferous in northern Tibet, knowledge on their faunal range and distribution and Jurassic biochronology remains questionable [32]. Jiang [36] named the rocks in Amdo 114 station as the Qiangmuleiqu Formation, which underlies of the Xushan Formation and overlies the Wenquan Formation of Middle Jurassic. Yong et al. [55] suggested that rocks at the station may be correlated with the Suowa Formation (also Upper Jurassic). The Qiangmuleiqu Formation is distinctly different from Yanshiping Group in the Qiantang basin in terms of lithology and fossils assemblages. In general, the Yanshiping Group in the northern Qiangtang is characterized by three sandstones horizons with two intercalated limestones horizons representing the continental or marginal-marine facies. In the light of abundant ammonites and bivalves, we confirm the strata at Amdo 114 station belong to middle to Late Tithonian (Late Jurassic).

*Depositional environment*

It is well-known that most areas of Qiangtang basin are shallow water environments from Late Triassic to Jurassic with carbonates and siliciclastic rocks showing episodic cycles [34, 56–57]. However, based on ammonites and cerium anomaly, present study shows that there may be stratigraphic sequence in the continental shelf with deep-water continental slope environments, or vice versa, which suggest the occurrence of deep water deposits in southern Qiangtang basin. As shown in Fig. 2, the eustatic sea-level began to rise in the lower part of the section until at about 390 m before reaching its maximum, then gradually fell near the reference sea-level with Ce anomaly of 0.1. As the observed three cycles could provide new insights for the sea-level changes, redox conditions, climatic and palaeogeographic events, further studies should be undertaken on Jurassic stratigraphic framework and tectono-sedimentary evolution in the Qiangtang basin of northern Tibet.

## Conclusions

The Upper Jurassic black rock series in the southern Qiangtang basin, northern Tibet contain ammonites of *Aulacosphinctes* and *Virgatosphinctes*

plus bivalves including *Buchia* and *Chlamys*, that are of Middle-Late Tithonian (Late Jurassic). The concentration of total REEs mainly range between 18.814 and 46.818 ppm and are lower than those of average shales. The shale-normalized [45] REE patterns are characterized by the flat-shale type with unstable Ce anomaly values of –0.238 to –0.015. Based on the $Ce_{anom}$ values, three cycles of eustatic sea-level changes were identified from the series. Changes in the positive anomalies would indicate a lowering of sea level as the apparent depth on the redox curve would reflect oxic conditions. Conversely, relative changes negative with time would indicate a rise in sea-level, as the apparent depth reflects anoxic conditions. Depending on the cerium anomalies and ammonites, we would suggest the Upper Jurassic black rock series in the southern Qiangtang basin exhibit alternative facies of the continental shelf with a deep-water continental slope, which is not consistent with the previous results.

## Acknowledgements

Thanks are extended to the Qinghai-Tibet research teams at Chengdu University of Technology for their kind help during our field investigation. We would like to thank Xixi Zhao, University of California (Santa Cruz) and two anonymous reviewers for their constructive reviews that improved the quality of the manuscript. This work was supported by National Natural Science Foundation of China (Grant No. 41102066, 40972084), Natural Science Foundation Project of CQ CSTC (Grant No. 2009BB7383), and Opening Foundation of the State Key Laboratory of Ore Deposit Geochemistry, Institute of Geochemistry, Chinese Academy of Sciences.

## REFERENCES

1. *Haq, B. U., Hardenbol, J., Vail, P. R.* // Science. 1987. Vol. 235, No. 4793. P. 1156–1167.
2. *Nakazawa, T., Ueno, K., Kawahata, H., Fujikawa, M., Kashiwagi, K.* Facies stacking patterns in high-frequency sequences influenced by long-term sea-level change on a Permian Panthalassan oceanic atoll: An example from the Akiyoshi Limestone, SW Japan // Sediment. Geol. 2009. Vol. 214, No.1–4. P. 35–48.
3. *Reolid, M., Nagy, J., Rodríguez-Tovar, F. J.* Ecostratigraphic trends of Jurassic agglutinated foraminiferal assemblages as a response to sea-level changes in shelf deposits of Svalbard (Norway) // Palaeogeogr. Palaeocl. 2010. Vol. 293, No. 1–2. P. 184–196.
4. *Brett, C. E., Baird, G. C., Bartholomew, A. J., De Santis, M. K., Ver Straeten, C. A.* Sequence stratigraphy and a revised sea-level curve for the Middle Devonian of eastern North America // Palaeogeogr. Palaeocl. 2011. Vol. 304, No. 1–2. P. 21–53.

5. *Ver Straeten, C. A., Brett, C. E., Sageman, B. B.* Mudrock sequence stratigraphy: A multi-proxy (sedimentological, paleobiological and geochemical) approach, Devonian Appalachian Basin // Palaeogeogr. Palaeocl. 2011. Vol. 304, No. 1–2. P. 54–73.
6. *Vail, P. R., Todd, R. G.* Northern North Sea Jurassic unconformities, chronostratigraphy and sea-level changes from seismic stratigraphy // Proc. Petroleum Geology of the Continental Shelf of North-West Europe Conf., March 4–6, 1980 / Illing, L. V., Hobson, G. D. (Eds.). London: Heydon, 1981. P. 216–235.
7. *Hallam, A.* A review of the broad pattern of Jurassic sea-level changes and their possible causes in the light of current knowledge // Palaeogeogr. Palaeocl. 2001. Vol. 167, No. 1–2. P. 23–37.
8. *Hesselbo, S. P.* Sequence stratigraphy and inferred relative sea-level change from the onshore British Jurassic // P. Geologists Assoc. 2008. Vol. 119, No. 1. P. 19–34.
9. *Glørstad-Clark, E., Faleide, J. I., Lundschien, B. A., Nystuen, J. P.* Triassic seismic sequence stratigraphy and paleogeography of the western Barents Sea area // Mar. Petrol. Geol. 2010. Vol. 27, No. 7. P. 1448–1475.
10. *Egenhoff, S., Cassle, C., Maletz, J., Frisk, Å. M., Ebbestad, J. O. R., Stübner, K.* Sedimentology and sequence stratigraphy of a pronounced Early Ordovician sea-level fall on Baltica-The Bjørkåsholmen Formation in Norway and Sweden // Sediment. Geol. 2010. Vol. 224, No. 1–4. P. 1–14.
11. *Nielsen, A. T., Schovsbo, N. H.* The Lower Cambrian of Scandinavia: Depositional environment, sequence stratigraphy and palaeogeography // Earth-Science Reviews. 2010. Vol. 107. No. 3–4. P. 207–310.
12. *Fielding, C. R., Browne, G. H., Field, B., Florindo, F., Harwood, D. M., Krissek, L. A., Levy, R. H., Panter, K. S., Passchier, S., Pekar, S. F.* Sequence stratigraphy of the ANDRILL AND-2A drillcore, Antarctica: A long-term, ice-proximal record of Early to Mid-Miocene climate, sea-level and glacial dynamism // Palaeogeogr. Palaeocl. 2011. Vol. 305, No. 1–4. P. 337–351.
13. *Van Daele, M., Van Welden, A., Moernaut, J., Beck, C., Audemard, F., Sanchez, J., Jouanne, F., Carrillo, E., Malavé, G., Lemus, A., De Batist, M.* Reconstruction of Late-Quaternary sea- and lake-level changes in a tectonically active marginal basin using seismic stratigraphy: The Gulf of Cariaco, NE Venezuela // Mar. Geol. 2011. Vol. 279, No. 1–4. P. 37–51.
14. *Wright, J., Schrader, H., Holser, W. T.* Paleoredox variations in ancient oceans recorded by rare earth elements in fossil apatite // Geochim. Cosmochim. Acta. 1987. Vol. 51, No. 3. P. 631–644.
15. *Wilde, P., Quinby-Hunt, M. S., Erdtmann, B.-D.* The whole-rock cerium anomaly: a potential indicator of eustatic sea-level changes in shales of the anoxic facies // Sediment. Geol, 1996. Vol. 101, No. 1–2. P. 43–53.
16. *Harding, I. C., Charles, A. J., Marshall, J. E. A., Pälike, H., Roberts, A. P., Wilson, P. A., Jarvis, E., Thorne, R., Morris, E., Moremon, R., Pearce, R. B., Akbari, S.* Sea-level and salinity fluctuations during the Paleocene-Eocene thermal maximum in Arctic Spitsbergen // Earth Planet. Sc. Lett. 2011. Vol. 303, No. 1–2. P. 97–107.
17. *Feng, H. Z., Erdtmann, B.-D., Wang, H. F.* Early Paleozoic whole-rock Ce anomalies and secular eustatic changes in the Upper Yangtze region // Sci. China Ser. D. 2000. Vol. 43, No. 3. P. 328–336.

18. *Shields, G., Stille, P.* Diagenetic constraints on the use of cerium anomalies as palaeoseawater redox proxies: an isotopic and REE study of Cambrian phosphorites // Chem. Geol. 2001. Vol. 175, No. 1–2. P. 29–48.
19. *Pattan, J. N., Pearce, N. J. G., Mislankar, P. G.* Constraints in using Cerium-anomaly of bulk sediments as an indicator of paleo bottom water redox environment: A case study from the Central Indian Ocean Basin // Chem. Geol. 2005. Vol. 221, No. 3–4. P. 260–278.
20. *Kakuwa, Y., Matsumoto, R.* Cerium negative anomaly just before the Permian and Triassic boundary event – The upward expansion of anoxia in the water column // Palaeogeogr., Palaeocl. 2006. Vol. 229, No. 4. P. 335–344.
21. *Class, C., le Roex, A. P.* Ce anomalies in Gough Island lavas – Trace element characteristics of a recycled sediment component // Earth Planet. Sc. Lett. 2008. Vol. 265, No. 3–4. P. 475–486.
22. *Tian, Y. L.* Ce anomaly as geochemical tracers for redox condition in carbonates of Sanya Formation, Qiongdongnan Basin // Offshore Oil. 2009. Vol. 30, No. 1. P. 21–25 [in Chinese with English abstract].
23. *Kerrich, R., Said, N.* Extreme positive Ce-anomalies in a 3.0 Ga submarine volcanic sequence, Murchison Province: Oxygenated marine bottom waters // Chem. Geol. 2011. Vol. 280, No. 1–2. P. 232–241.
24. *Schulte, P., Scheibner, C., Speijer, R. P.* Fluvial discharge and sea-level changes controlling black shale deposition during the Paleocene-Eocene Thermal Maximum in the Dababiya Quarry section, Egypt // Chem. Geol. 2011. Vol. 285, No. 1–4. P. 167–183.
25. *Liu, Y.-G., Miah, M. R. U., Schmitt, R. A.* Cerium: A chemical tracer for paleo-oceanic redox conditions // Geochem. Cosmochim. Acta. 1988. Vol. 52, No. 6. P. 1361–1371.
26. *Kato, Y., Nakao, K., Isozaki, Y.* Geochemistry of Late Permian to Early Triassic pelagic cherts from southwest Japan: implications for an oceanic redox change // Chem. Geol. 2002. Vol. 182, No. 1. P. 15–34.
27. *Girard, C., Lécuyer, C.* Variations in Ce anomalies of conodonts through the Frasnian/Famennian boundary of Poland (Kowala – Holy Cross Mountains): implications for the redox state of seawater and biodiversity // Palaeogeogr., Palaeocl. 2002. Vol. 181, No. 1. P. 299–311.
28. *Murray, R. W., Buchholtz ten Brink, M. R., Jones, D. L., Gerlach, D. C., Price Russ, G.* Rare earth elements as indicators of different marine depositional environments in chert and shale // Geology. 1990. Vol. 18, No. 3. P. 268–271.
29. *Elderfield, H., Greaves, M. J.* The rare earth elements in seawater // Nature. 1982. Vol. 296. P. 214–219.
30. *Wilde, P.* Model of progressive ventilation of the late Precambrian-early Paleozoic Ocean // Am. J. Sci. 1987. Vol. 287. P. 442–459.
31. *Li, Y. T., Luo, J. N., Lu, H. N., Xu, W. K., Tong, Z. Y., Wu, R. Z.* Qianghai-Tibet Stratigraphy. – Beijing: Science Publishing House, 2001. P. 1–400 [in Chinese].
32. *Yin, J. R., Enay, R.* Tithonian ammonoid biostratigraphy in eastern Himalayan Tibet // Geobios-Lyon. 2004. Vol. 37, No. 5. P. 667–686.
33. *Yin, J. R., Sun, L. X, Bai, Z. D., Xu, D. B., Zhang, X. J.* New data on the Jurassic ammonites from the Shuanghu and Amdo areas, with comments on the Jurassic strata in north Tibet // Journal of Stratigraphy. 2005. Vol. 29, No. 1. P. 7–15 [in Chinese with English abstract].
34. *Yi, H. S., Wang, C. S., Lin, J. H., Shi, Z. Q., Chen, L., Wu, X. H., Wei, Q. L., Zhang, X. Q.* Jurassic ammonite fauna in the Amdo area, northern Tibet and its

paleogeographic implications // Geological Bulletin of China. 2005. Vol. 24, No. 1. P. 41–47 [in Chinese with English abstract].
35. *Chen, L., Yi, H. S., Zhong, H., Hu., R. Z., Yin, J. R., Yang, J. K.* The calcareous nannofossils record and its geological significance in the Jurassic black shales from the Qiangtang Basin, northern Tibetan Plateau // Prog. Nat. Sci. 2006. Vol. 16, Supplement 1. P. 264–273.
36. *Jiang, Z. T.* The problems of Jurassic stratigraphy in Qiangtang district. In CGOXP Editorial Committee Ministry of Geology and Mineral Resources PRC. Contribution to the geology of the Qinghai-Xizang (Tibet) Plateau (No. 3). – Beijing: Geological Publishing House, 1983. P. 87–112 [in Chinese].
37. *Enay, R.*, *Cariou, E.* Ammonite faunas and palaeobiogeography of the Himalayan belt during the Jurassic: Initiation of a Late Jurassic austral ammonite fauna // Palaeogeogr. Palaeocl. 1997. Vol. 134, No. 1–4. P. 1–38.
38. *Cecca, F.* Palaeobiogeography of Tethyan ammonites during the Tithonian (latest Jurassic) // Palaeogeogr. Palaeocl. 1999. Vol. 147, No. 1–2. P. 1–37.
39. *Oloriz, F.*, *Tintori, A.* Upper Jurassic (Tithonian) ammonites from the Spiti Shales in Western Zanskar (NW Himalayas) // Riv. Ital. Paleontol. S. 1990. Vol. 96. No. 4. P. 461–486.
40. *Yin, J. R., Fürsich, F. T.* Dispersal events of Triassic-Jurassic boundary faunas, and paleoenvironment of Tibetan Himalaya // Sci. China Ser. D. 2009. Vol. 52, No. 12. P. 1993–2000.
41. *Pearce, N. J. G., Perkins, W. T., Westgate, J. A., Gorton, M. P., Jackson, S. E., Neal, C. R., Chenery, S. P.* A compilation of new and published major and trace element data for NIST SRM 610 and NIST SRM 612 glass reference materials // Geostandard. Newslett. 1997. Vol. 21, No. 1. P. 115–144.
42. *Westgate, J. A., Shane, P. A. R., Pearce, N. G. J., Perkins, W. T., Korisettar, R., Chesner, C. A.,Willams, M. A., Acharyya, S. K.* All Toba tephra occurrences across peninsular India belong to the 75000 yr B.P. eruption // Quaternary Res. 1998. Vol. 50, No. 1. P. 107–112.
43. *Liang, Q., Jing, H., Grégoire, D. C.* Determination of trace elements in granites by inductively coupled plasma mass spectrometry // Talanta. 2000. Vol. 51, No. 3. P. 507–513.
44. *Turekian, K. K., Wedepohl, K. H.* Distribution of the elements in some major units of the earth's crust // Geol. Soc. Am. Bull. 1961. Vol. 72, No. 2. P. 175–192.
45. *McLennan, S. M.* Rare earth elements in sedimentary rocks; influence of provenance and sedimentary processes // Rev. Mineral. Geochem. 1989. Vol. 21, No. 1. P. 169–200.
46. *Mazumdar, A., Banerjee, D. M., Schidlowski, M., Balaram, V.* Rare-earth elements and stable isotope geochemistry of early Cambrian chert–phosphorite assemblages from the Lower Tal Formation of the Krol Belt (Lesser Himalaya, India) // Chem. Geol. 1999. Vol. 156, No. 1–4. P. 275–297.
47. *Morad, S., Felitsyn, S.* Identification of primary Ce-anomaly signatures in fossil biogenic apatite: implication for the Cambrian oceanic anoxia and phosphogenesis // Sediment. Geol. 2001. Vol. 143, No. 3–4. P. 259–264.
48. *Bau, M., Dulski, P.* Distribution of yttrium and rare-earth elements in the Penge and Kuruman iron-formations, Transvaal Suergroup, South Africa // Precambrian Res. 1996. Vol. 79, No. 1–2, P. 37–55.
49. *Taylor, S. R., McLennan, S. M.* The Continental Crust: its Composition and Evolution. – Oxford: Blachwell, 1985. pp. 312.

50. *Guo, Q. J., Shields, G. A., Liu, C. Q., Strauss, H., Zhu, M. Y., Pi, D. H., Goldberg, T., Yang, X. L.* Trace element chemostratigraphy of two Ediacaran-Cambrian successions in South China: Implications for organosedimentary metal enrichment and silicification in the early Cambrian // Palaeogeogr. Palaeocl. 2007. Vol. 254, No. 1–2. P. 194–216.
51. *Yang, J. D., Sun, W. G., Wang, Z. Z., Xue, Y. S., Tao, X. C.* Variations in Sr and C isotopes and Ce anomalies in successions from China: evidence for the oxygenation of Neoproterozoic seawater? // Precambrian Res. 1999. Vol. 93, No. 2–3. P. 215–233.
52. *Yin, J. R., Wan, X. Q.* Jurassic ammonite morphotypes as water-depth indicator of Tethys-Himalaya sea // Acta of Palaeontological Sinica. 1996. Vol. 35, No. 6. P. 734–751 [in Chinese with English abstract].
53. *Hallam, A.* A re-evaluation of Jurassic eustasy in the light of new data and the revised Exxon curve // Wilgus, C. K., Hastings, B. S., Kendall, C. G. St. C., Posamentier, H. W., Ross, C. A., van Wagoner, J. C. (Eds.) / Sea-Level Changes: An Integrated Approach. - SEPM Special Publication, 1988. Vol. 42. P. 261–273.
54. *Fan, H. P., Yang, J. Q., Zhang, P.* Late Jurassic strata in northern Tibet // Journal of Stratigraphy. 1988. Vol. 12, No. 1. P. 66–70 [in Chinese].
55. *Yong, Y. Y., Luo, J. N., Yu, Q.* Report of investigation on petroleum geology in the Eastern Manalaiqin-Shuijinkuan-Xijinwulanhu area, Qiangtang basin (Internal data). 1995 [in Chinese].
56. *Fu, X. G., Wang, J., Qu, W. J., Duan, T. Z., Du, A. D., Wang, Z. J., Liu, H.* Re-Os (ICP-MS) dating of marine oil shale in the Qiangtang basin, Northern Tibet, China // Oil Shale. 2008. Vol. 25. No. 1. P. 47–55.
57. *Fu, X. G., Wang, J., Tan, F. W., Zeng, Y. H.* Sedimentological investigations of the Shengli River-Changshe Mountain oil shale (China): relationships with oil shale formation // Oil Shale. 2009. Vol. 26. No. 3. P. 373–381.

*Presented by V. Kalm*
Received March 16, 2011